ORIGINAL ARTICLE

JBMR

Inhibition of Sclerostin by Monoclonal Antibody Enhances Bone Healing and Improves Bone Density and Strength of Nonfractured Bones

Michael S Ominsky,[1] Chaoyang Li,[1] Xiaodong Li,[1] Hong L Tan,[1] Edward Lee,[1] Mauricio Barrero,[1] Franklin J Asuncion,[1] Denise Dwyer,[1] Chun-Ya Han,[1] Fay Vlasseros,[2] Rana Samadfam,[2] Jacquelin Jolette,[2] Susan Y Smith,[2] Marina Stolina,[1] David L Lacey,[1] William S Simonet,[1] Chris Paszty,[1] Gang Li,[3] and Hua Z Ke[1]

[1]Metabolic Disorders, Amgen Inc., Thousand Oaks, CA, USA
[2]Bone Research, Preclinical Services, Charles River Laboratories, Montreal, Quebec, Canada
[3]Stem Cell and Regeneration Program, Li Ka Shing Institute of Health Sciences, School of Biomedical Sciences and Department of Orthopaedics and Traumatology, Chinese University of Hong Kong, Hong Kong, SAR China

ABSTRACT

Therapeutic enhancement of fracture healing would help to prevent the occurrence of orthopedic complications such as nonunion and revision surgery. Sclerostin is a negative regulator of bone formation, and treatment with a sclerostin monoclonal antibody (Scl-Ab) results in increased bone formation and bone mass in animal models. Our objective was to investigate the effects of systemic administration of Scl-Ab in two models of fracture healing. In both a closed femoral fracture model in rats and a fibular osteotomy model in cynomolgus monkeys, Scl-Ab significantly increased bone mass and bone strength at the site of fracture. After 10 weeks of healing in nonhuman primates, the fractures in the Scl-Ab group had less callus cartilage and smaller fracture gaps containing more bone and less fibrovascular tissue. These improvements at the fracture site corresponded with improvements in bone formation, bone mass, and bone strength at nonfractured cortical and trabecular sites in both studies. Thus the potent anabolic activity of Scl-Ab throughout the skeleton also was associated with an anabolic effect at the site of fracture. These results support the potential for systemic Scl-Ab administration to enhance fracture healing in patients. © 2011 American Society for Bone and Mineral Research.

KEY WORDS: FRACTURE HEALING; SCLEROSTIN; SCLEROSTIN ANTIBODY; WNT; STRENGTH

Introduction

Fracture healing is a complex biologic process involving inflammation, granulation, callus formation, and bone modeling/remodeling.[1] Optimal fracture healing results in complete restoration of bone structure and function to the prefracture levels. However, some fractures are associated with a high risk of delayed union, nonunion, and other complications. Overall, 5% to 10% of all fractures result in impaired healing or nonunion, creating a significant public health problem.[2] Currently, there are device therapies such as bone morphogenetic proteins (BMPs) that have been used to treat these types of fracture-associated complications.[2,3] Additionally, BMPs have been used to facilitate bone healing in acute open tibial diaphyseal fractures and lumbar spinal fusion in skeletally mature patients with degenerative disk disease.[4] BMPs must be implanted surgically with a carrier at the site of fracture to have their therapeutic effect, which limits their use to surgeries with open access to the fracture site. In addition, the degree of clinical benefit may not outweigh the high cost of BMPs,[5] and their use may result in complications such as local bone resorption, heterotopic bone formation, or edema.[6] To date, there is no noninvasive, systemic therapy to facilitate fracture healing and reduce the risk of fracture-associated complications such as nonunion and revision surgery.

Recently, it has been suggested that canonical Wnt signaling plays an important role in fracture healing.[7] Expression of various Wnts has been reported to be upregulated during

Received in original form August 4, 2010; revised form October 13, 2010; accepted November 18, 2010. Published online December 2, 2010.
Address correspondence to: Michael S Ominsky, PhD, Bone and Mineral Metabolism, Department of Metabolic Disorders, Amgen Inc., One Amgen Center Drive, MS 15-2-A, Thousand Oaks, CA 91320, USA. E-mail: mominsky@amgen.com
Parts of the article were presented at the 31st Annual Meeting of the American Society for Bone and Mineral Research, Denver, CO, September 11–15, 2009, and the IOF World Congress on Osteoporosis & 10th European Congress on Clinical and Economic Aspects of Osteoporosis and Osteoarthritis, Florence, Italy, May 5–8, 2010.
Additional Supporting Information may be found in the online version of this article.

Journal of Bone and Mineral Research, Vol. 26, No. 5, May 2011, pp 1012–1021
DOI: 10.1002/jbmr.307

fracture repair, and increased β-catenin signaling by lithium administration has been shown to improve fracture healing.[8] Conversely, inhibition of the Wnt/β-catenin pathway by adenoviral overexpression of Dickkopf 1 has been shown to inhibit the fracture healing process.[8–10] These results suggest that agents that activate the Wnt/β-catenin signaling pathway may have the potential to improve fracture healing.

Sclerostin, a protein secreted primarily by osteocytes, is a negative regulator of osteoblast differentiation/function and acts as an inhibitor of bone formation.[11–14] Humans with inherited sclerostin deficiency (sclerosteosis or van Buchem disease) have increased bone mass and are resistant to fracture.[15,16] Sclerostin knockout mice have greater bone mass and bone strength owing to increased bone formation.[17] Although the mechanism by which sclerostin negatively regulates bone formation is an area of continuing investigation, one body of research supports the hypothesis that sclerostin binds to LRP5/6 to inhibit Wnt/β-catenin signaling,[18] thus impairing osteoblast differentiation and function. Sclerostin antibodies (Scl-Abs) have been shown to neutralize the inhibitory effects of sclerostin on Wnt/β-catenin signaling in vitro[19,20] and to have significant bone anabolic activity in various species in vivo. Treatment with a murine Scl-Ab significantly increased bone formation on trabecular, periosteal, endocortical, and intracortical bone surfaces in a rat model of osteoporosis, leading to an increase in bone mass and bone strength.[20] Similarly, treatment with a humanized Scl-Ab resulted in increased bone formation, bone mass, and bone strength in intact nonhuman primates[21] and increased biochemical markers of bone formation in healthy men and postmenopausal women.[22]

This study investigated the effects of systemic administration of Scl-Ab in two models used previously to assess the effects of therapeutic agents on fracture healing: the rat closed femoral fracture model[23] and the cynomolgus monkey fibular osteotomy model.[24] We hypothesized that Scl-Ab would enhance fracture healing in these models by increasing bone formation, bone mass, and bone strength at the site of fracture, in addition to its anabolic effects at nonfractured sites.

Materials and Methods

The animal studies were conducted in Association for Assessment and Accreditation of Laboratory Animal Care (AAALAC)–accredited facilities in accordance with federal animal care guidelines, and the protocols were approved by the Amgen Institutional Animal Care and Use Committee. The nonhuman primate study was performed at Charles River Laboratories (Montreal, Quebec, Canada).

Rat closed femoral fracture model

Male Sprague-Dawley (SD) rats (7 to 7.5 months old, mean body weight of 580 g) were assigned to receive vehicle ($n = 18$) or Scl-AbIII ($n = 17$). Scl-AbIII was generated by ratizing a mouse sclerostin antibody to reduce the likelihood of the molecule being cleared by the rat immune system. Unilateral closed femoral mid-diaphyseal fractures were created based on the previously reported model.[23] Briefly, an 18-gauge syringe needle was inserted into the medullary canal through the condyles. The femur then underwent transverse fracture via blunt impact loading at the anterior (lateral) aspect of the thigh. One day after the fracture, rats were injected subcutaneously with either saline vehicle or Scl-Ab at 25 mg/kg twice per week for 7 weeks. A postoperative radiograph is provided for illustrative purposes in Fig. 1*A*. Radiographs were taken weekly to monitor the progress of the healing (LX 60; Faxitron, Inc., Wheeling, IL, USA). Three rats from the Scl-Ab group with radiographic evidence of poorly aligned, unstable fractures within the first week were removed from the study, reducing the number to 14. After 7 weeks, the rats were euthanized, and blood was collected by cardiac puncture. The bone-formation markers N-terminal propeptide of procollagen type 1 (P1NP) and

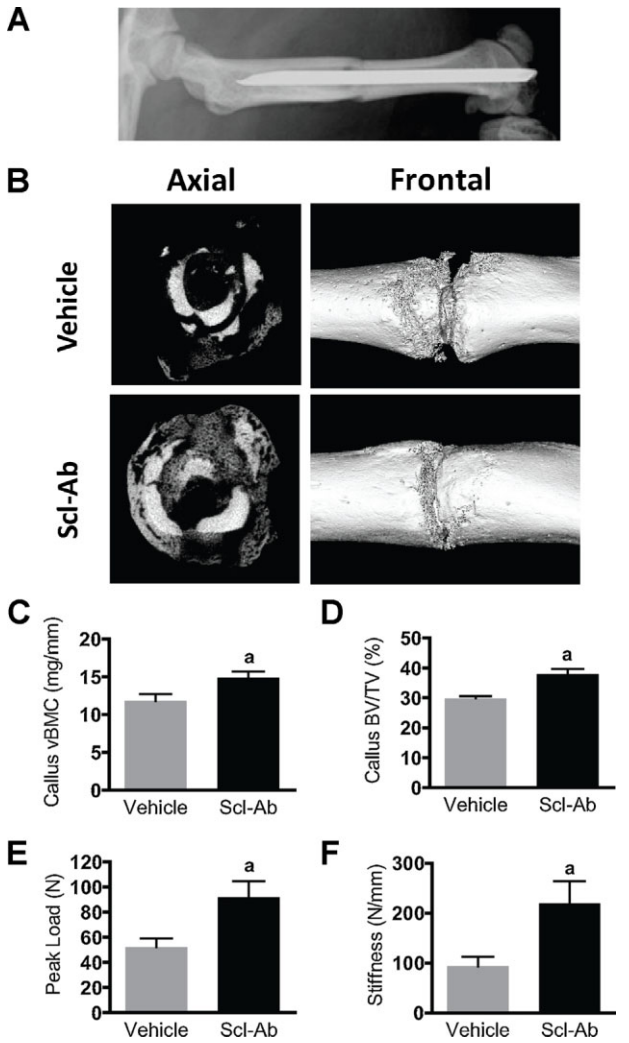

Fig. 1. Systemic administration of Scl-Ab increased bone mass and strength in the rat closed femoral fracture callus. (*A*) A radiograph of the stabilized closed femoral fracture immediately after fracture. (*B*) Representative axial and frontal μCT images at the fracture site after 7 weeks of twice-weekly subcutaneous injections of vehicle or 25 mg/kg of Scl-Ab. (*C*, *D*) Scl-Ab increased BMC and bone volume/total volume (BV/TV), as determined from μCT scans of the central 1-mm region of the callus excluding the original cortex. (*E*, *F*) Peak load and stiffness were significantly increased in the Scl-Ab-treated fractured femurs, as determined by destructive three-point bending test. Data are expressed as mean ± SE; $n = 14$ to 18/group. $^{a}p < .05$ versus vehicle. μCT images represent the group medians for peak load.

osteocalcin were assessed in the terminal serum by ELISA (IDS, Fountain Hills, AZ, USA) or Luminex-based assay (Millipore, St Charles, MO, USA), respectively. At termination, both fractured and nonfractured contralateral femurs were collected, the intramedullary pins were removed, and the femurs were stored at −20°C prior to ex vivo densitometry and bone strength testing. Femurs were scanned ex vivo by dual-energy X-ray absorptiometry (DXA; PIXImus II; GE Lunar, Madison, WI, USA) at the fracture region (middle 30% of the femur) or the corresponding region in the contralateral femur to determine areal bone mineral density (aBMD). Both femurs also were scanned using a desktop micro–computed tomographic (μCT) system (eXplore Locus SP; GE Healthcare, London, Ontario, Canada) and reconstructed to a resolution of 30 μm. The area, bone mineral content (BMC), and BMD of the central 1 mm of the fracture callus were assessed after subtraction of the original cortex, as described previously.[25] Callus bone volume as a percent of total volume (BV/TV) was quantified using a variable threshold (480 to 700 mg/cm^3), with higher thresholds applied to the denser calluses based on qualitative examination of callus architecture. For the intact contralateral femur, regions spanning 10% of the femur height at the midshaft (threshold 800 mg/cm^3) and trabecular distal femur (threshold 450 mg/cm^3 for vehicle and 550 mg/cm^3 for Scl-Ab) were examined. Unthresholded volumetric BMC was assessed at these sites and in a 0.13-mm-thick region at the femoral neck. Femurs were tested in three-point bending to failure at the center of the fracture callus or at the contralateral midshaft, and bone-strength parameters were assessed (MTS 858 Mini Bionix II, MTS Systems Corp., Eden Prairie, MN, USA; span length = 20 mm, displacement rate = 0.1 mm/s).

Nonhuman primate fibular osteotomy model

After a 6-week acclimation period, 4- to 5-year-old male cynomolgus monkeys (mean body weight 6.4 kg, range 5.1 to 7.7 kg) were assigned to receive either vehicle ($n = 21$) or Scl-Ab (humanized Scl-AbV, $n = 22$). Surgical osteotomies were performed bilaterally at the midshaft of each fibula based on a previously reported model.[24,26] Briefly, a single transverse osteotomy was made through the fibular midshaft, and a stainless steel Kirschner wire (K-wire; ranging from 0.027 to 0.062 mm in diameter) was passed down the medullary canal from the midshaft through the distal aspect of the fibula. The bisected fibula was realigned, and the intramedullary pin was passed retrograde through the proximal half to stabilize the osteotomy. A postoperative radiograph is provided for illustrative purposes in Fig. 2*A*. After surgery, the animals were immediately allowed full weight-bearing activity on becoming ambulatory. One day after surgery, animals were injected subcutaneously with vehicle (10 mM sodium acetate, 9% sucrose, 0.004% polysorbate 20, pH 5.2) or Scl-Ab (30 mg/kg) every 2 weeks for 10 weeks at an injection volume of 0.43 mL/kg. Serum was collected every 2 weeks for assessment of drug concentrations (ELISA; Amgen Inc.) and the bone-resorption marker C-telopeptide (CTX; Serum Crosslaps ELISA; Nordic Biosciences, Copenhagen, Denmark). Bone densitometry was assessed in vivo using a DXA scanner (Hologic Discovery A, Hologic, Inc., Waltham, MA, USA) at baseline and prior to termination at 10 weeks. The fluorescent label tetracycline (25 mg/kg) was infused intravenously at 2 and 3.5 weeks following surgery; bicarbonate-buffered calcein (8 mg/kg) was infused intravenously after 8 and 9.5 weeks. At termination, lumbar vertebrae (L_3, L_4) and the left fibula were wrapped in saline-soaked gauze and frozen at −20°C prior to biomechanical testing. The L_2 vertebra, femoral neck, central femur, and right fibula were placed in 10% neutral buffered formalin for 3 days and then postfixed in 70% ethanol prior to embedding for histomorphometric analysis. When left fibulas were obviously bent or otherwise damaged, right fibulas were allotted to biomechanical testing. Four animals in the Scl-Ab group were

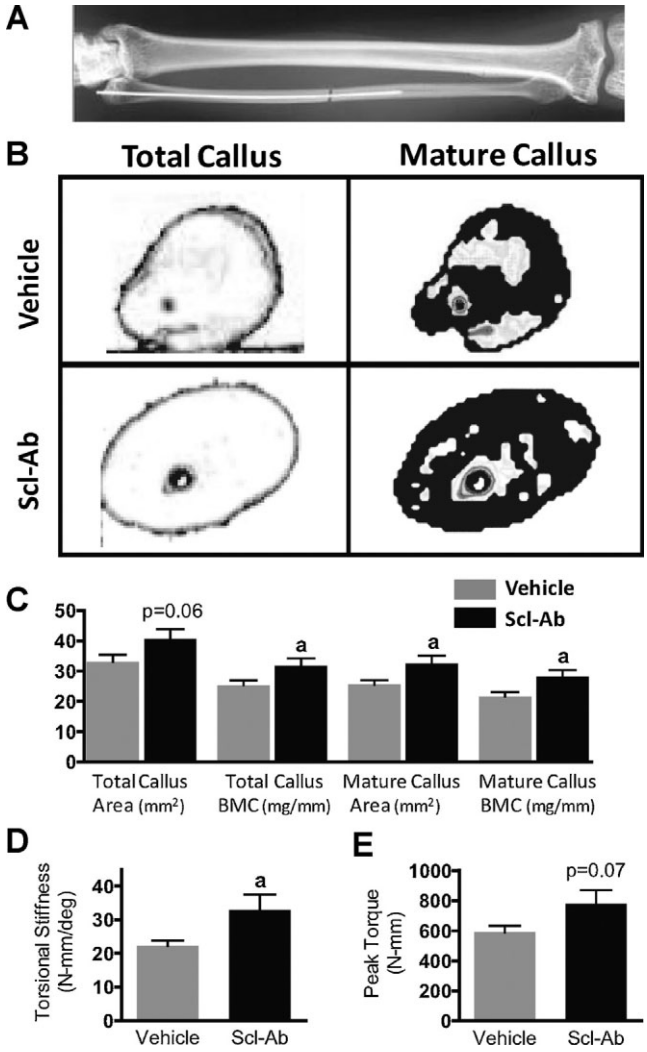

Fig. 2. Systemic administration of Scl-Ab increased the bone mass and strength of the callus in a nonhuman primate fibular osteotomy model. (*A*) A radiograph of the stabilized fibular osteotomy immediately after fracture. (*B*) Representative axial pQCT images through the osteotomy site after 10 weeks of vehicle or Scl-Ab treatment. The black regions in the mature callus image represent the more dense regions within the total callus (density > 1090 cm^{-1}). (*C*) Quantification of area and BMC from the pQCT scans demonstrated significant improvements in total callus BMC, mature callus area, and mature callus BMC with Scl-Ab treatment. (*D*) Torsional stiffness and (*E*) peak torque were increased in the Scl-Ab-treated fibular osteotomies, as determined by destructive torsion testing. Data are expressed as mean ± SE; $n = 12$ to 17/group. [a]$p < .05$ versus vehicle.

excluded from all analyses owing to undetectable drug levels in their serum by week 6, presumably due to the formation of neutralizing antibodies to Scl-Ab.

Fractured bone analyses

The K-wires were removed from the fractured fibulas prior to analysis by peripheral quantitative computed tomography (pQCT) and strength assessment in torsion. Faxitron X-ray images were taken before and after pin removal to confirm that the pins were removed completely, that no damage occurred during the pin removal process, and that the fibulas were aligned adequately for torsional testing. Six fibulas were excluded (3 vehicle, 3 Scl-Ab) owing to significant bending in the intramedullary pin, which generally was evident in the in vivo radiographs by week 2. In addition, exclusions were made for one vehicle-treated fibula owing to a broken pin, one Scl-Ab-treated fibula that separated during pin removal, and two Scl-Ab-treated fibulas that were pinned improperly. The remaining 17 vehicle- and 12 Scl-Ab-treated fibulas were scanned at the osteotomy midpoint 1 mm proximal and 1 mm distal to the midpoint. Total area, BMC, and BMD data were generated using an outer edge detection of 1090 cm^{-1} (cortmode 2), and mature callus area, BMC, and BMD were calculated using a threshold of 1090 cm^{-1} (peelmode 2; XCT Research SA, Pforzheim, Germany). The ends of the fibulas were potted in square molds using methyl methacrylate, resulting in a span length of 55 mm (coefficient of variation = 2.0%). The fibulas were tested counterclockwise to failure at 1.5 degrees/s using the MTS 858 Mini-Bionix servohydraulic test system, and peak torque and torsional stiffness were recorded. Five additional specimens in the vehicle-treated group were excluded from the torsion results, three owing to separation during the potting/testing process and two owing to a fracture at the site where the intramedullary pin pierced the outer cortex. Exclusions for nonseparated fibulas were made by a biomechanical expert based on the load-displacement curves and X-rays after a blinded review. Thus the strength data from 12 fibulas per group are reported below.

Histologic analysis was performed on the available right fibulas from the first 10 animals of each group that were not excluded owing to drug clearance or fibular abnormalities, as described earlier. Fibulas were dehydrated and embedded undecalcified in methyl methacrylate with the pin in situ; longitudinal sections were cut, ground, and stained with Stevenel's blue. The region spanning 6 mm on either side of the osteotomy was scored semiquantitatively in a blinded manner from 0 (none) to 5 (severe) for incomplete union, fracture gap width, the extent of cartilage in the external callus, and the extent of bone in the gap between the original fractured cortices. Incomplete union scoring criteria were 0 = full osseous callus and cortical bridging; 1 = mainly osseous callus bridging with scant cartilage in one side; 2 = mainly osseous callus bridging with a small amount of cartilage and fibrovascular tissue between cortices; 3 = mixed bone and cartilage callus bridging, along with some fibrovascular tissue between cortices; 4 = minimal osseous callus bridging and extensive fibrovascular tissue between cortices; 5 = no osseous callus bridging and extensive fibrovascular tissue between cortices. Subsequent histomorphometric analysis was performed to quantify the external size and composition (ie, bone, cartilage, and fibrovascular tissue) of the external callus and internal fracture gap further (Image-Pro Plus Image Analyzer, Version 6.3, Media Cybernetics, Inc., Bethesda, MD, USA). One fibula in the vehicle-treated group was excluded from analysis owing to severe suppurative inflammation and bone loss at the site of fracture, reducing the number to 9.

Nonfractured bone analyses

The end plates and spinous processes from L_3 and L_4 vertebral bodies were removed using a diamond saw to obtain a specimen with planoparallel ends of approximately 8 mm in height. The vertebral bodies were compressed to failure at 20 mm/min, and peak load, stiffness, and energy to failure (area under the load-displacement curve) were calculated.

Histomorphometry was performed on the L_2 vertebra, right femoral midneck, and right femoral midshaft from the 10 animals in each group assessed for fibular histology. Tissues were dehydrated and embedded in methyl methacrylate without decalcification. For L_2, sagittal sections were examined by histomorphometry for static (5 μm thick, Goldner's trichrome) and dynamic (7 μm thick, unstained) parameters in the cancellous region, respectively. Thick transverse sections at the femoral neck were ground and stained with Stevenel's blue for static cancellous parameters or left unstained for dynamic histomorphometry. At the femoral midshaft, unstained transverse sections were ground for evaluation of both static and dynamic cortical parameters. Dynamic histomorphometric parameters for all sites included mineralizing surface (MS/BS), mineral apposition rate (MAR), and bone-formation rate (BFR/BS), as described elsewhere.[27]

Statistical analyses

Statistical analyses were performed in GraphPad Prism (Version 5.01, GraphPad Software, Inc., San Diego, CA, USA) for the rat study and SAS (Version. 8.1, SAS Institute, Inc., Cary, NC, USA) for the nonhuman primate study. Group variances were compared by *F* test (rat) or Levene's test (nonhuman primate). If the group variances were significantly heterogeneous ($p < .05$), the data were log-transformed and resubmitted to assess the variance. When differences between group variances were not significant, a parametric two-sample *t* test was used to perform the group mean comparisons between the vehicle- and Scl-Ab-treated groups. When group variances remained heterogeneous ($p < .05$), the comparison was conducted using the Mann-Whitney test (rat) or Wilcoxon rank-sum test (nonhuman primate).

Results

Scl-Ab increased biomechanical strength in a rat closed femoral fracture model

Seven weeks of Scl-Ab administration increased skeletal bone formation, as demonstrated by a 21% increase in serum P1NP (16.0 ± 4.0 ng/mL versus 13.2 ± 0.8 ng/mL in vehicle, $p < .05$) and a 14% increase in serum osteocalcin (90.0 ± 4.6 ng/mL versus 79.1 ± 2.1 ng/mL in vehicle, $p < .05$). The increase in bone-

formation markers with Scl-Ab corresponded with greater bone mass in the central 30% of the fractured rat femur, as demonstrated by increases of 19% and 11% in BMC and BMD, respectively, measured by DXA compared with vehicle after 7 weeks ($p < .05$ for both; data not shown). In Fig. 1*B*, representative μCT images through the fracture line (axial 2D section) and of the entire fracture region (frontal 3D rendered view) illustrate the increases in bone mass in this region. μCT analysis of the central 1-mm region of the fracture demonstrated that Scl-Ab significantly increased callus cross-sectional area (+14%, $40.7 \pm 1.3\,mm^2$ versus $35.6 \pm 1.6\,mm^2$) and callus volumetric BMC (+26%; Fig. 1*C*) compared with vehicle-treated controls (both $p < .05$). Threshold analysis demonstrated that callus BV/TV was 41% greater after Scl-Ab treatment than after vehicle treatment ($p < .05$; Fig. 1*D*). The increased bone mass in the Scl-Ab-treated callus corresponded to a 60% increase in peak load and a 149% increase in stiffness, as determined by destructive three-point bend testing compared with vehicle (both $p < .05$; Fig. 1*E*, *F*).

In the intact contralateral femur, Scl-Ab was effective at increasing BMC in the trabecular distal femur, femoral neck, and cortical midshaft (Table 1). These anabolic increases in BMC were associated with significant increases in cortical and trabecular thickness in the midshaft and distal femur, respectively, after Scl-Ab treatment (both $p < .05$ versus vehicle). The Scl-Ab-mediated increase in cortical bone resulted in a 17% greater peak bending load in the Scl-Ab group compared with vehicle ($p < .05$). Thus, under these conditions, Scl-Ab increased bone mass and strength of both intact and fractured bones in rats.

After 7 weeks, fractures in the vehicle- and Scl-Ab-treated groups healed to 27% and 48% of the mean peak load of intact contralateral femurs in the vehicle-treated group. There was a fivefold increase in the percentage of fractures treated with Scl-Ab that had a peak load greater than 50% of the vehicle-treated contralateral mean (36% versus 6% for vehicle-treated fractured femurs, $p < .05$), reflecting a significant improvement in the rate that the majority of intact strength was recovered.

Scl-Ab enhanced fracture healing in a nonhuman primate fibular osteotomy model

Ten weeks of systemic Scl-Ab administration resulted in greater bone mass in fractured fibulas by pQCT when compared with vehicle-treated controls ($p < .05$; Fig. 2*C*). Threshold analysis demonstrated that there was a greater amount of mature callus area (+27%) and BMC (+30%) in the Scl-Ab-treated group than in the vehicle-treated group (both $p < .05$), as illustrated in black within the representative pQCT images from each group in Fig. 2*B*. The increase in callus bone mass with Scl-Ab treatment was associated with improved bone strength, as demonstrated by a 48% increase in torsional stiffness ($p < .05$) and a 32% increase in peak torque ($p = .07$) compared with vehicle (Fig. 2*D*, *E*).

Histology demonstrated the variable response in bone healing at this site, as shown in Fig. 3*A*. These images illustrate the range of size and tissue composition of the external callus and fracture gap between the cortices in both groups. Semiquantitative analysis (on a scale from 0 to 5) demonstrated that there was a significant reduction in incomplete union score in the Scl-Ab-treated group (Fig. 3*B*). Nonzero values for incomplete union were observed in 5 of 9 fractures in the vehicle-treated group and only 1 of 10 fractures in the Scl-Ab-treated group. This change corresponded to nonsignificant reductions in the extent of cartilage in the callus and fracture gap size with Scl-Ab and a significant increase in the extent of bone in the fracture gap ($p < .05$ versus vehicle). Thus the healing process in Scl-Ab-treated fibulas was advanced more consistently than in the vehicle-treated group. Subsequent quantitative histomorphometry of the fracture region demonstrated similar improvements in histologic fracture healing, as demonstrated by significant reductions in callus cartilage and fracture gap area with Scl-Ab (Fig. 3*C*). The smaller fracture gaps in the Scl-Ab-treated group tended to contain more bone and less fibrovascular tissue than in the vehicle-treated group (both $p < .10$). Three of the 9 fracture gaps in the vehicle-treated controls contained more than 50% fibrovascular tissue volume compared with 0 of 10 in the Scl-Ab-treated group. These histologic results are consistent with the finding that a greater number of fibulas in the vehicle-treated group (3) than in the Scl-Ab-treated group (1) came apart at the fracture line in preparation for biomechanically testing.

Table 1. Scl-Ab Increased Bone Mass and Strength in the Intact Rat Femur

μCT/strength endpoint	Units	Vehicle	Scl-Ab
Distal femur Tb.vBMC	mg/mm	3.07 ± 0.15	$4.26 \pm 0.31^*$
Distal femur Tb.BV/TV	%	16.4 ± 3.8	$23.1 \pm 2.0^*$
Distal femur Tb.Th	μm	56.5 ± 1.4	$97.4 \pm 2.7^*$
Femoral neck vBMC	mg/mm	3.23 ± 0.08	$3.68 \pm 0.14^*$
Femoral diaphysis Ct.vBMC	mg/mm	9.10 ± 0.23	$10.05 \pm 0.29^*$
Femoral diaphysis Ct.Th	μm	838 ± 19	$922 \pm 18^*$
Femoral diaphysis peak load	N	191 ± 8	$223 \pm 10^*$
Femoral diaphysis stiffness	N/mm	570 ± 22	637 ± 37

Mean ± SE. Tb = trabecular; Ct = cortical; vBMC = volumetric bone mineral content; BV/TV = bone volume/total volume, Th = thickness.
$^*p < .05$ versus vehicle, $n = 14$ to 18/group.

Scl-Ab increased bone mass, bone strength, and bone formation in the nonfractured, nonhuman primate skeleton

Ten weeks of systemic administration of Scl-Ab resulted in significant increases in DXA-determined BMD throughout the skeleton, including sites that are prone to osteoporotic fracture in humans (ie, lumbar spine, total hip, and distal radius; Table 2). The greatest BMD increments were observed at the lumbar spine, and histomorphometry demonstrated that Scl-Ab increased bone formation (Fig. 4*A*, *B*) and bone volume (Fig. 4*D*) in the second lumbar (L_2) vertebra. The 48% increase in L_2 trabecular bone volume in the Scl-Ab-treated group was associated with increases of 158% and 111% in bone-formation rates, as assessed at the beginning (weeks 2 to 3.5) and end of the study (weeks 8 to 9.5), respectively. The augmented lumbar vertebrae were stronger, as demonstrated by a 30% increase in peak compressive load in L_3 and L_4 vertebrae after only 10 weeks of Scl-Ab administration ($p < .05$ versus vehicle; Fig. 4*E*).

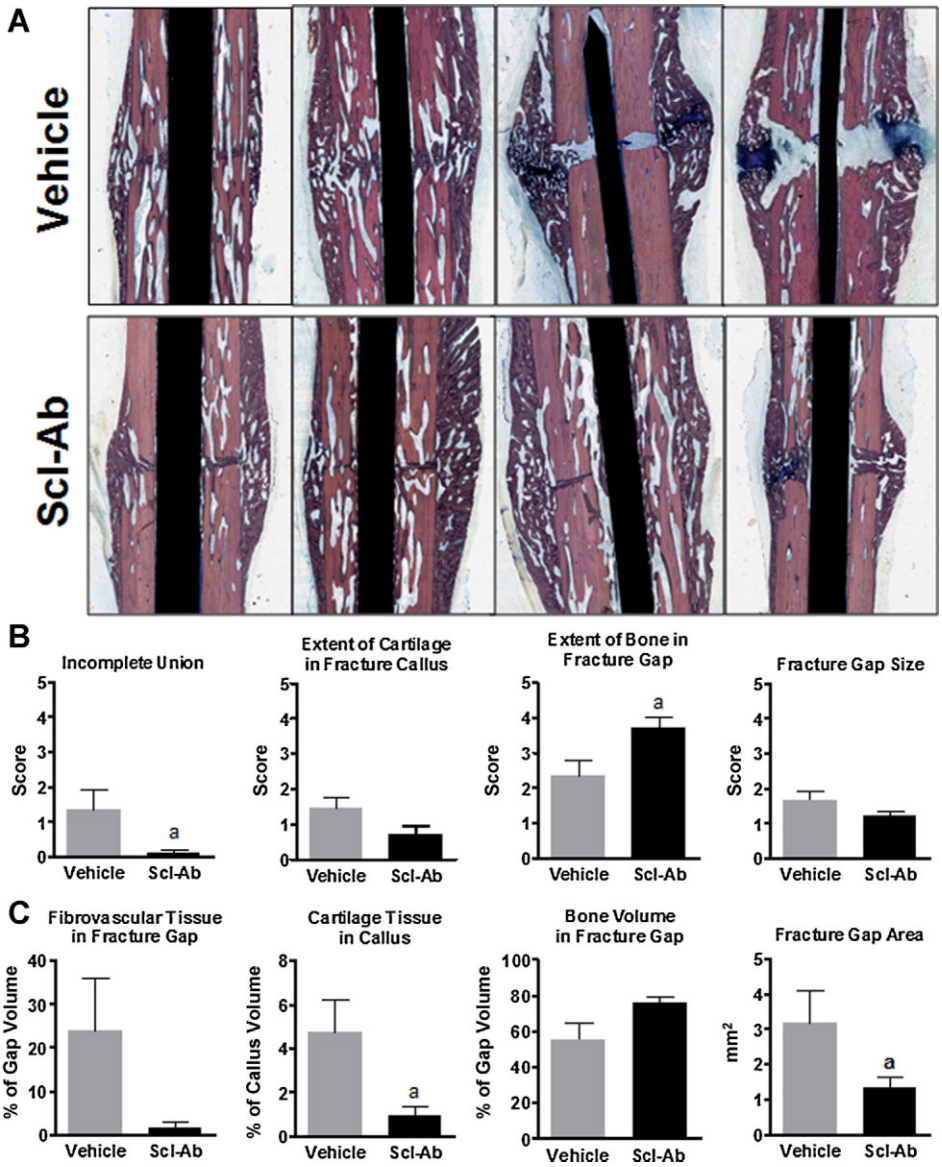

Fig. 3. Systemic administration of Scl-Ab improved histologic bone healing in nonhuman primates. (*A*) Representative longitudinal (Stevenel's blue–stained) sections demonstrating the range of healing responses at the fibular osteotomy in the vehicle- ($n = 9$) and Scl-Ab-treated ($n = 10$) groups. (*B*) Semiquantitative scoring was performed to evaluate the progress to healing, as reflected in the lack of complete fracture union, the extent of cartilage in the fracture callus, the extent of bone in the fracture gap, and the size of the fracture gap. Each section was scored on a scale from 0 (not apparent) to 5 (severe) in a blinded manner. (*C*) Histomorphometry was performed to further quantify these parameters, including percent fibrovascular tissue in the fracture gap, percent cartilage tissue in the callus, percent bone in the fracture gap, and total area of the fracture gap. Data are expressed as mean ± SE. [a] $p < .05$ versus vehicle.

Table 2. Scl-Ab Increased BMD Throughout the Nonhuman Primate Skeleton

DXA aBMD site (% change from baseline)	Vehicle	Scl-Ab	Difference
Total hip	9.3 ± 1.5	14.5 ± 1.8	+5.2*
Femoral neck	7.6 ± 2.1	17.4 ± 1.6	+9.8*
1/3 Distal radius	3.3 ± 0.6	5.6 ± 0.9	+2.2*
Lumbar spine	4.4 ± 0.5	16.6 ± 1.2	+12.2*

Mean ± SE.
*$p < .05$ versus vehicle, $n = 17$ to 21/group.

Scl-Ab treatment also resulted in higher bone-formation rates in the trabecular region of the femoral neck and in the cortex of the femoral diaphysis (Table 3). The increase in trabecular bone formation with Scl-Ab corresponded with significant increases in trabecular thickness at both the L_2 vertebra (+51%, 172 ± 14 μm versus 114 ± 5 μm) and femoral neck (+28%; Table 3). Newly formed bone in Scl-Ab-treated animals was confirmed to have normal lamellar structure, and accumulation of woven bone was not observed at these sites. The Scl-Ab-mediated increase in bone formation was not associated with increases in histologic indices of bone resorption. Eroded surface and osteoclast surface were significantly or numerically lower at both the L_2 vertebra

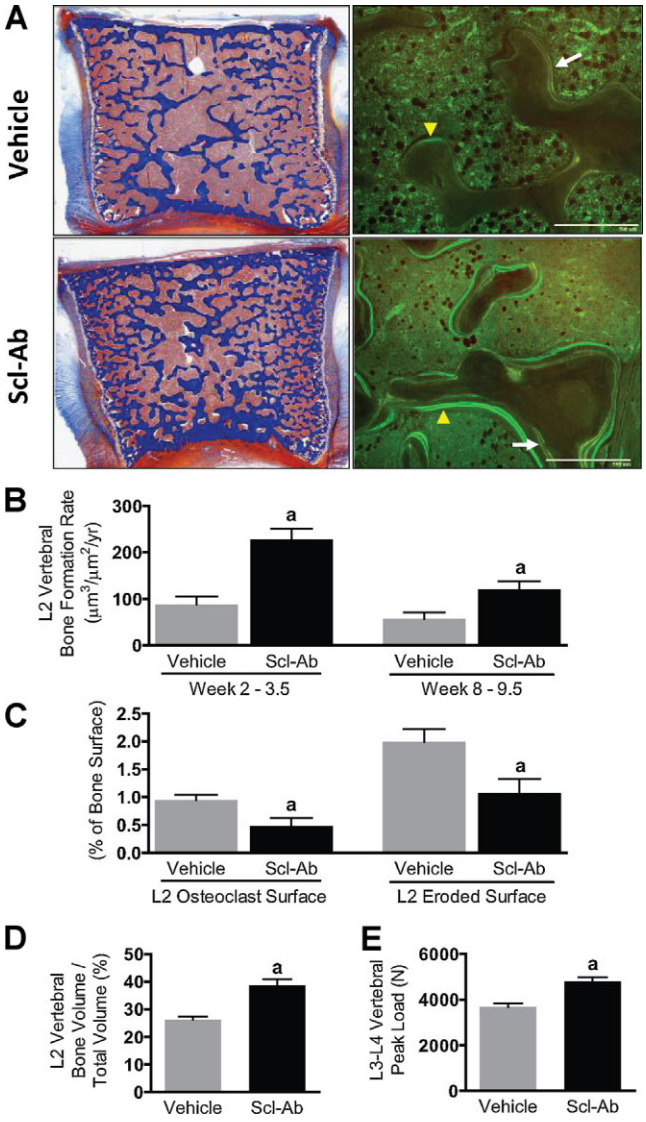

Fig. 4. Systemic administration of Scl-Ab increased bone formation, bone volume, and bone strength at the lumbar vertebra in nonhuman primates. (*A*) Representative sagittal sections of the second lumbar vertebral body (L_2) from the vehicle- and Scl-Ab-treated groups ($n = 10$/group). The left panel contains images taken from Goldner's trichrome–stained sections with a ×10 objective; the right panel contains epifluorescent images taken from unstained sections with a ×40 objective (white bars = 500 μm). Tetracycline (*yellow label*, shown with *white arrows*) was administered after 2 and 3.5 weeks of treatment; calcein (*green label*, shown with *yellow arrowheads*) was administered after 8 and 9.5 weeks. (*B*) Scl-Ab increased bone-formation rate, as determined for each set of double labels in the trabecular compartment of L_2. (*C*) The bone-resorption parameters osteoclast surface and eroded surface (as a percent of bone surface) were decreased significantly after 10 weeks of Scl-Ab treatment. (*D*) L_2 trabecular bone volume/total volume also was increased significantly by Scl-Ab. (*E*) L_3 and L_4 vertebral bodies were compressed to failure, and Scl-Ab treatment resulted in a significant increase in mean peak load (data expressed as an average of L_3 and L_4, $n = 18$ to 21/group). Data are expressed as mean ± SE. $^a p < .05$ versus vehicle.

and the femoral neck after Scl-Ab treatment (Fig. 4*C* and Table 3). In addition, Scl-Ab did not increase cortical porosity at the femoral midshaft (Table 3). These results suggest that local increases in bone resorption are not required for the increased bone formation observed with Scl-Ab treatment.

Discussion

This study provides the first evidence that inhibition of sclerostin via systemic antibody administration can enhance fracture healing in animal models. In both the rat and nonhuman primate fracture healing models, Scl-Ab increased callus size, bone mass, and bone strength at the fracture site. Without additional time points, it is unclear whether this increase in callus cross-sectional area was a consequence of greater periosteal bone formation, greater initial callus formation, or changes in callus remodeling. Based on the nonhuman primate histology and densitometry data, the Scl-Ab-treated fracture calluses were more mature, containing less cartilage and more dense bone. Although it is not yet clear whether Scl-Ab had any direct effects on the formation or removal of cartilage, sclerostin expression has been detected in hypertrophic chondrocytes in human tissue.[14] The development of a cartilaginous callus depends in part on the amount of motion at the fracture site, with a transition to bone once the fracture has been stabilized sufficiently.[1] Thus, if Scl-Ab resulted in an earlier stabilization of the fracture, it should result in a more mature callus by the end of the study. Evidence for a more consistently stabilized fracture was observed between the ends of the osteotomy, where the Scl-Ab-treated fracture gaps were smaller and contained less fibrovascular tissue and more bone. The increased bone formed in the gap may be directly related to the effects of reversing sclerostin's inhibitory effect on osteoblast activity. Although the mechanism by which Scl-Ab decreased the size of the fracture gap is unclear, it likely resulted from a decrease in bone resorption at the fractured ends. This apparent decrease in resorption may have resulted indirectly via an earlier stimulation of bone formation on the fractured surfaces.

The observation that Scl-Ab resulted in less frequent incomplete histologic union in nonhuman primates and a greater rate of achieving 50% of intact strength in rats supports the potential of systemic inhibition of sclerostin to improve healing outcomes. In the United States alone, over 6 million adults per year experience fractures,[28] with certain fractures more highly associated with poor outcomes (eg, nonunion, malunion, revision surgery, and reduced function). Thus a therapeutic agent that improves outcomes could have important clinical benefits. In addition, most fractures are managed nonoperatively[29]; therefore there is a great need for a noninvasive systemic therapy that could accelerate healing in these settings. The temporal effects of Scl-Ab on the composition and progression of healing fractures will be the subject of future studies.

The healing response in the 7- to 7.5-month-old vehicle-treated rats was less than typically reported in a closed femoral fracture model in younger rats (such as rats 9 to 12 weeks old), which are generally well healed within 7 weeks. This finding is consistent with other reports that fracture healing slows with rodent age.[30] The 7- to 7.5-month-old rat closed femoral fracture model provided a more challenging model for an anabolic therapy, without the potential influence of age-

Table 3. Scl-Ab Increased Bone Formation at the Femoral Neck and Femoral Diaphysis in Nonhuman Primates

Histomorphometry endpoint	Units	Vehicle	Scl-Ab
FN BV/TV	%	27.5 ± 2.3	33.6 ± 2.1
FN Tb.Th	μm	152 ± 12	$194 \pm 6^*$
FN osteoclast surface/BS	%	0.33 ± 0.08	0.26 ± 0.09
FN eroded surface/BS	%	1.95 ± 0.33	0.86 ± 0.19
FN Tb.BFR/BS (weeks 2 to 3.5)	$\mu m^3/\mu m^2/yr$	44.8 ± 8.0	$157.6 \pm 20.1^*$
FN Tb.BFR/BS (weeks 8 to 9.5)	$\mu m^3/\mu m^2/yr$	62.4 ± 12.1	100.4 ± 17.9
FD cortical area	mm^2	54.7 ± 2.0	56.0 ± 6.7
FD cortical porosity	%	1.13 ± 0.10	0.99 ± 0.07
FD Ps.BFR/BS (weeks 2 to 3.5)	$\mu m^3/\mu m^2/yr$	79.3 ± 15.8	$187 \pm 36^*$
FD Ec.BFR/BS (weeks 2 to 3.5)	$\mu m^3/\mu m^2/yr$	50.5 ± 14.8	$238 \pm 42^*$
FD Ps.BFR/BS (weeks 8 to 9.5)	$\mu m^3/\mu m^2/yr$	6.4 ± 3.4	15.0 ± 5.2
FD Ec.BFR/BS (weeks 8 to 9.5)	$\mu m^3/\mu m^2/yr$	35.5 ± 10.6	$270 \pm 37^*$

Mean ± SE. FN = femoral neck ($n = 8$/group); FD = femoral diaphysis ($n = 10$/group); BV/TV = bone volume/total volume; Tb = trabecular; BS = bone surface; BFR = bone-formation rate; Ps = periosteal; Ec = endocortical; Th = thickness.

$^*p < .05$ versus vehicle.

dependent increases in bone mass and longitudinal bone growth. In the adolescent primates, the healing response in vehicle-treated controls after 10 weeks was more complete, with incomplete union rarely observed and callus area and strength slightly less than that reported previously in older primates.[24] The maximum torque of the fractured fibulas in the vehicle-treated group in this study was similar to that in intact fibulas taken from a set of 8 similarly aged primates (590 ± 41 N · mm versus 527 ± 42 N · mm).

As a systemic therapy, Scl-Ab in this study also increased bone formation, bone mass, and/or bone strength at the nonfractured sites of the lumbar spine and proximal femur, at which osteoporotic fractures occur frequently. After an initial osteoporotic fracture, patients are at greater risk of subsequent fracture.[31] Patients experiencing these secondary osteoporotic fractures have a greater incidence of death.[32] Therefore, an anabolic therapy that increases bone strength throughout the skeleton while improving fracture healing should reduce the risk of a secondary osteoporotic fracture. In male rats, Scl-Ab increased serum markers of bone formation, as well as bone mass and strength of the femoral midshaft, similar to a previous report in aged ovariectomized (OVX) rats.[20] Increases in bone mass in the femoral neck and trabecular distal femur also were observed. This study in male cynomolgus monkeys provided a larger sample size ($n = 18$ to 21/group) to evaluate the skeletal effects of Scl-Ab in a remodeling species, complementing the anabolic effects reported previously in female cynomolgus monkeys ($n = 2$ to 4/group).[21] Scl-Ab significantly increased DXA-determined BMD at the lumbar spine, total hip, femoral neck, and distal radius. The increase in lumbar spine BMD was associated with significant improvement in peak compressive load of the lumbar vertebrae. In the subset of nonhuman primates with tissues collected for histomorphometry, the vertebral bodies and femoral neck had thicker trabeculae, presumably owing to the increase in bone-formation rate at these sites. At the cortical midshaft, Scl-Ab increased bone formation on the periosteal and endocortical surfaces. The anabolic effect was less pronounced on the periosteal surface, and the decrease in BFR/BS in both groups during the study suggested that the surgery may have resulted in transient changes in periosteal bone formation independent of treatment. Consistent with the previous reports of the effects of Scl-Ab in rats[20] and cynomolgus monkeys,[21] bone formed during Scl-Ab treatment in this study was of normal lamellar architecture with no evidence of woven bone accumulation.

Despite the significant increases in bone formation at all sites, Scl-Ab did not result in increased histologic bone resorption at any site. Scl-Ab decreased osteoclast surface and eroded surface in trabecular bone, and no effect of treatment was observed on femoral midshaft cortical porosity. These results differ from the anabolic effects of intermittent parathyroid hormone (PTH), which were associated with dose-dependent increases in cortical porosity in older OVX nonhuman primates.[33,34] Although the mechanism by which Scl-Ab reduced osteoclastic resorption is unclear, similar evidence for an antiresorptive effect with Scl-Ab administration was observed in OVX rats[20] and in healthy men and postmenopausal women.[22] However, inconsistent with the changes in histologic resorption, serum CTX was significantly increased in the Scl-Ab group at the end of the study (3.2 ± 0.3 ng/mL versus 2.5 ± 0.1 ng/mL, $p < .05$). An increase in serum CTX with Scl-Ab was not observed previously in female nonhuman primates[21] and may have been related to increased bone turnover at the fracture site and the greater callus size in the Scl-Ab group. Patients with tibia fractures were reported to have greater postfracture increases in serum CTX than patients with smaller malleolar fractures.[35] The effects of Scl-Ab on bone resorption require additional investigation and may depend on species and/or context.

Currently, no systemic therapy has been approved to enhance fracture healing in patients. Intermittent PTH, an approved anabolic therapy in osteoporosis, has been shown to improve skeletal repair in the rat closed femur fracture model[36,37] but failed to achieve its primary goal of improved time to radiographic healing in a prospective, placebo-controlled clinical trial in patients with radial fractures.[38] Intermittent PTH improved callus remodeling but did not increase whole-femur

strength in a femur osteotomy model in adult cynomolgus monkeys,[39] although the time point examined was well after the initial healing phase (26 weeks). Whether the improvements in bone strength in the rat and primate fracture models with Scl-Ab will result in improved fracture outcomes in humans is the subject of ongoing clinical trials.

In summary, inhibition of sclerostin by systemic administration of Scl-Ab increased bone formation, bone mass, and bone strength in fractured and nonfractured bones in rat and nonhuman primate models of fracture healing. These results support the potential of Scl-Ab as an attractive noninvasive strategy to enhance fracture healing. Furthermore, Scl-Ab may have the potential to prevent secondary fractures in other skeletal sites in osteoporotic fracture patients owing to its ability to increase bone formation, bone mass, and bone strength in nonfractured bones.

Disclosures

MSO, CYL, XL, HLT, EL, MB, FJA, MS, DW, CYH, DLL, WSS, CP, and HZK are employees of and own stock in Amgen Inc. Charles River Laboratories and GL received funding from Amgen Inc.

Acknowledgments

We thank the members of the Amgen Inc. and UCB, Inc. sclerostin teams for their support of these studies. We also thank Charles Turner from Indiana University for his careful evaluation of the biomechanical testing data from the primate study. Michelle N Bradley provided editorial support on behalf of Amgen Inc.

References

1. Zuscik M, O'Keefe RJ. Skeletal healing. In: Rosen CJ, ed. *Primer on the Metabolic Bone Diseases and Disorders of Mineral Metabolism*. Washington, DC: American Society for Bone and Mineral Research, 2008:61–65.
2. Einhorn TA. Enhancement of fracture-healing. J Bone Joint Surg Am. 1995;77:940–956.
3. Einhorn TA. Clinical applications of recombinant human BMPs: early experience and future development. J Bone Joint Surg Am. 2003; 85:S82–88.
4. Mont MA, Ragland PS, Biggins B, et al. Use of bone morphogenetic proteins for musculoskeletal applications: an overview. J Bone Joint Surg Am. 2004;86:S41–55.
5. Garrison KR, Donell S, Ryder J, et al. Clinical effectiveness and cost-effectiveness of bone morphogenetic proteins in the non-healing of fractures and spinal fusion: a systematic review. Health Technol Assess. 2007;11:1–150, iii-iv.
6. Poynton AR, Lane JM. Safety profile for the clinical use of bone morphogenetic proteins in the spine. Spine (Phila Pa 1976). 2002; 27:S40–48.
7. Secreto FJ, Hoeppner LH, Westendorf JJ. Wnt signaling during fracture repair. Curr Osteoporos Rep. 2009;7:64–69.
8. Chen Y, Whetstone HC, Lin AC, et al. Beta-catenin signaling plays a disparate role in different phases of fracture repair: implications for therapy to improve bone healing. PLoS Med. 2007;4:e249.
9. Kim JB, Leucht P, Lam K, et al. Bone regeneration is regulated by wnt signaling. J Bone Miner Res. 2007;22:1913–1923.
10. Leucht P, Kim JB, Helms JA. Beta-catenin-dependent Wnt signaling in mandibular bone regeneration. J Bone Joint Surg Am. 2008;90 (Suppl 1): 3–8.
11. Balemans W, Ebeling M, Patel N, et al. Increased bone density in sclerosteosis is due to the deficiency of a novel secreted protein (SOST). Hum Mol Genet. 2001;10:537–543.
12. Brunkow ME, Gardner JC, Van Ness J, et al. Bone dysplasia sclerosteosis results from loss of the SOST gene product, a novel cystine knot-containing protein. Am J Hum Genet. 2001;68:577–589.
13. Poole KE, van Bezooijen RL, Loveridge N, et al. Sclerostin is a delayed secreted product of osteocytes that inhibits bone formation. FASEB J. 2005;19:1842–1844.
14. Winkler DG, Sutherland MK, Geoghegan JC, et al. Osteocyte control of bone formation via sclerostin, a novel BMP antagonist. EMBO J. 2003;22:6267–6276.
15. Hamersma H, Gardner J, Beighton P. The natural history of sclerosteosis. Clin Genet. 2003;63:192–197.
16. Vanhoenacker FM, Balemans W, Tan GJ, et al. Van Buchem disease: lifetime evolution of radioclinical features. Skeletal Radiol. 2003; 32:708–718.
17. Li X, Ominsky MS, Niu QT, et al. Targeted deletion of the sclerostin gene in mice results in increased bone formation and bone strength. J Bone Miner Res. 2008;23:860–869.
18. Baron R, Rawadi G. Targeting the Wnt/beta-catenin pathway to regulate bone formation in the adult skeleton. Endocrinology. 2007;148:2635–2643.
19. Veverka V, Henry AJ, Slocombe PM, et al. Characterization of the structural features and interactions of sclerostin: molecular insight into a key regulator of Wnt-mediated bone formation. J Biol Chem. 2009;284:10890–10900.
20. Li X, Ominsky MS, Warmington KS, et al. Sclerostin antibody treatment increases bone formation, bone mass, and bone strength in a rat model of postmenopausal osteoporosis. J Bone Miner Res. 2009; 24:578–588.
21. Ominsky MS, Vlasseros F, Jolette J, et al. Two doses of sclerostin antibody in cynomolgus monkeys increases bone formation, bone mineral density, and bone strength. J Bone Miner Res. 2010;25:948–959.
22. Padhi D, Jang G, Stouch B, et al. Single-dose, placebo-controlled, randomized study of AMG 785, a sclerostin monoclonal antibody. J Bone Miner Res. 2011;26:19–26.
23. Bonnarens F, Einhorn TA. Production of a standard closed fracture in laboratory animal bone. J Orthop Res. 1984;2:97–101.
24. Seeherman HJ, Bouxsein M, Kim H, et al. Recombinant human bone morphogenetic protein-2 delivered in an injectable calcium phosphate paste accelerates osteotomy-site healing in a nonhuman primate model. J Bone Joint Surg Am. 2004;86-A:1961–1972.
25. Taylor DK, Meganck JA, Terkhorn S, et al. Thrombospondin-2 influences the proportion of cartilage and bone during fracture healing. J Bone Miner Res. 2009;24:1043–1054.
26. Seeherman H, Li R, Bouxsein M, et al. rhBMP-2/calcium phosphate matrix accelerates osteotomy-site healing in a nonhuman primate model at multiple treatment times and concentrations. J Bone Joint Surg Am. 2006;88:144–160.
27. Parfitt AM, Drezner MK, Glorieux FH, et al. Bone histomorphometry: standardization of nomenclature, symbols, and units. Report of the ASBMR Histomorphometry Nomenclature Committee. J Bone Miner Res. 1987;2:595–610.
28. Court-Brown CM, Koval KJ. The epidemiology of fractures. In: Bucholz RW, Heckman JD, Court-Brown CM, eds. *Rockwood and Green's Fractures in Adults*. Philadelphia, PA, USA: Lippincott, 2006: 96–143.
29. Court-Brown CM, Aitken S, Hamilton TW, et al. Nonoperative Fracture Treatment in the Modern Era. J Trauma. 2010;69:699–707.

30. Meyer RA, Tsahakis PJ, Martin DF, et al. Age and ovariectomy impair both the normalization of mechanical properties and the accretion of mineral by the fracture callus in rats. J Orthop Res. 2001;19:428–435.
31. Center JR, Bliuc D, Nguyen TV, et al. Risk of subsequent fracture after low-trauma fracture in men and women. JAMA. 2007;297:387–394.
32. Bliuc D, Nguyen ND, Milch VE, et al. Mortality risk associated with low-trauma osteoporotic fracture and subsequent fracture in men and women. JAMA. 2009;301:513–521.
33. Burr DB, Hirano T, Turner CH, et al. Intermittently administered human parathyroid hormone(1-34) treatment increases intracortical bone turnover and porosity without reducing bone strength in the humerus of ovariectomized cynomolgus monkeys. J Bone Miner Res. 2001;16:157–165.
34. Fox J, Miller MA, Newman MK, et al. Effects of daily treatment with parathyroid hormone 1-84 for 16 months on density, architecture and biomechanical properties of cortical bone in adult ovariectomized rhesus monkeys. Bone. 2007;41:321–330.
35. Stoffel K, Engler H, Kuster M, et al. Changes in biochemical markers after lower limb fractures. Clin Chem. 2007;53:131–134.
36. Nakajima A, Shimoji N, Shiomi K, et al. Mechanisms for the enhancement of fracture healing in rats treated with intermittent low-dose human parathyroid hormone (1-34). J Bone Miner Res. 2002;17:2038–2047.
37. Tagil M, McDonald MM, Morse A, et al. Intermittent PTH((1-34)) does not increase union rates in open rat femoral fractures and exhibits attenuated anabolic effects compared to closed fractures. Bone. 2010;46:852–859.
38. Aspenberg P, Genant HK, Johansson T, et al. Teriparatide for acceleration of fracture repair in humans: a prospective, randomized, double-blind study of 102 postmenopausal women with distal radial fractures. J Bone Miner Res. 2010;25:404–414.
39. Manabe T, Mori S, Mashiba T, et al. Human parathyroid hormone (1-34) accelerates natural fracture healing process in the femoral osteotomy model of cynomolgus monkeys. Bone. 2007;40:1475–1482.